Quantum Electronics **49** (6) 545–551 (2019) ©2019 Kvantovaya Elektronika and Turpion Ltd

https://doi.org/10.1070/QEL17036

Electronic and optical properties of hybrid GaN/por-Si(111) heterostructures

P.V. Seredin, D.L. Goloshchapov, D.S. Zolotukhin, A.S. Lenshin, A.M. Mizerov, I.N. Arsent'ev, H. Leiste, M. Rinke

Abstract. **Using plasma-assisted molecular beam epitaxy (PA MBE) of nitrogen, we obtained integrated heterostructures based on a self-ordered array of GaN nanocolumns on Si substrates with a sufficiently uniform distribution of diameters, which subsequently coalesced into a 2D layer. The use of a 'compliant' por-Si substrate for GaN synthesis using PA MBE allowed us to obtain a crack-free GaN layer, prevent the Ga-Si etching process, maintain a sharp smooth Si–GaN interface, and also partially suppress the generation of tensile stresses caused by cooling the heterostructure from growth temperature to room temperature by its relaxation at the Si–GaN nanoporous interface, which had a positive effect on its optical properties in the UV region.**

Keywords: *gallium nitride, nanocolumns, molecular beam epitaxy, porous silicon, optical and electronic properties.*

1. Introduction

Today, great efforts are being made all over the world to study various approaches to the integration of optical functional elements and silicon circuitry for processing electrical signals [1–3]. This problem is due to the ever-increasing demands for developing a new generation of elements of the optoelectronic component base with a much higher throughput and lower power consumption than the currently existing optoelectronic counterparts, i.e., the development of 'silicon photonics' is needed, designed to embed sources and receivers of radiation on a silicon substrate [4]. In addition, this is related to the search for alternatives to sapphire and silicon carbide based substrates.

Over the past decades, many approaches have been proposed to improve the crystal perfection of heterostructures based on the III–N system of materials [5]. However, the impressive difference between the lattice constants and the thermal expansion coefficients of solid solutions of AIIIN nitrides and a Si substrate seriously complicates the growth of good-quality operating heterostructures, leading to a variety of defects in the waveguides of devices, such as cracking, uncontrollable composition fluctuations during epitaxial growth of solid solutions and, finally, to a significant reduction in the device efficiency [6].

Among the many possible approaches to solving the described problems arising from the integration of AIIIN and Si, only a few have now been studied that allow combining AIIIN semiconductor materials and a silicon chip, such as epitaxial growth on transition (buffer) layers for filtering dislocations intergrowing from the heterointerface to the active region of the device heterostructure [7, 8], growth through gradient layers and the use of SiGe technology [9].

Considering the approaches to epitaxial growth on the transition (buffer) layers of the AIIIN/Si structures, we should note that multi-period superlattices, layers with alternating 2D and 3D morphology, layers with a smooth change are used to filter dislocations that grow from the heterointerface to the active region of the device heterostructure composition, etc., as well as their combinations [7, 8, 10]. The buffer layers are complex, multilayer heterostructures, the thickness of which can reach several tens of micrometres. In this case, the heterogeneity of the composition of the buffer layers limits the possibility of their use as a waveguide for acoustic waves when fabricating acoustoelectronic devices. In addition, despite the fact that the use of buffer layers can effectively reduce the density of intergrowing dislocations in the active zone of the heterostructure, their density at the AIIIN/Si heterointerface remains high, deteriorating the acoustic properties of the final structure. As for the development of SiGe technology, its use is justified only in the particular case of producing silicon-germanium electronics, for which the difference in lattice parameters in a Ge/Si heteropair is minimal, which greatly simplifies epitaxial growth and removes a number of problems.

After the appearance of the first GaN/Si LEDs [11] and the release of commercial products based on them, the main line of exploratory research in world practice, aimed at solving the problems of the AIIIN/Si-technology, is the development of monolithic integrated hybrid AIIIN/Si heterostructures for making microdiode arrays capable of supporting a high signal modulation rate and integrated optoelectronic reception and transmission systems on a chip [12]. As recent studies in this area have shown, in the case of successfully overcoming the problems facing this technology, devices derived from such hybrid integration will dominate the market [13–15].

The development of technology of AIIIN and silicon hybrid integration promises a radical change in our understanding of

P.V. Seredin Voronezh State University, Universitetskaya pl. 1, 394006 Voronezh, Russia; Ural Federal University named after the first President of Russia B.N. Yeltsin, ul. Mira 19, 620002 Ekaterinburg, Russia; e-mail: paul@phys.vsu.ru;
D.L. Goloschapov, D.S. Zolotukhin, A.S. Lenshin Voronezh State University, Universitetskaya pl. 1, 394006 Voronezh, Russia;
A.M. Mizerov St. Petersburg Academic University, Russian Academy of Sciences, ul. Khlopina 8, korp. 3A, 194021 St. Petersburg, Russia;
I.N. Arsent'ev Ioffe Institute, Russian Academy of Sciences, ul. Politekhnicheskaya 26, 194021 St. Petersburg, Russia;
H. Leiste, M. Rinke Karlsruhe Nano Micro Facility H.-von-Helmholtz-Platz 1, 76344 Eggenstein-Leopoldshafen, Germany

Received 4 April 2019
Kvantovaya Elektronika **49** (6) 545–551 (2019)
Translated by V.L. Derbov

the future photonics, which is associated primarily with the fabrication of one-dimensional nanoheterostructures. Heteroepitaxy in one-dimensional form (nanowire/nanocolumn) makes it possible to integrate various materials that are not easy to grow together in the form of thin films, to use a variety of new material combinations in a single heteropair. It also provides an ideal platform for the subsequent manufacture of hybrid heterostructures combining the best transport and optical characteristics of dissimilar materials in one device [16, 17].

Reducing the elastic energy arising due to the mismatch of the lattice parameters by producing a layer of nanocolumns and their subsequent coalescence may play an important role in the further growth of the low-defect AIIIN single-crystal film on them.

In the majority of papers devoted to the formation of nanocolumn structures, the authors use two main approaches. First, the IIIIN nanocolumns are grown with their subsequent coalescence by gas phase epitaxy from organometallic compounds (GPEOMC) on previously masked Si substrates, which are necessary for nucleation of the nanocolumn layers [18]. Second, plasma-assited molecular beam epitaxy (PA MBE) of nitrogen produces IIII nanocolumns, after which the coalescence of nanocolumns into a continuous layer is provided by the GPEOMC method [19].

However, despite the emerging progress, the search for more optimal ways to integrate AIIIN and Si continues. The main reason for this is the problem of low dislocation and low-defect growth of the epitaxial layer on silicon, which is not completely solved. In the literature, there is still no information on approaches to the effective reduction of elastic energy arising from the inconsistency of the lattice parameters during the growth of hybrid heterostructures by creating a layer of nanocolumns and their subsequent coalescence. In addition, the search continues for technological methods, which make it possible to obtain hybrid heterostructures with high functional characteristics. These difficulties have not yet been overcome, but the development of new approaches to the epitaxial growth of nitrides on Si substrates using molecular beam epitaxy has already improved the quality of the film obtained on the crystalline Si substrate to the level corresponding to the possibility of active use in optoelectronics.

In our opinion, one of the ways to efficiently manage elastic energy in epitaxial growth processes of IIII/Si hybrid heterostructures, and, consequently, to improve the performance of final devices, is to use 'compliant' Si substrates, which are a nanoporous silicon layer and formed on it epitaxial structure with 3D (in the form of nanocolumns) morphology [20–22]. In our previous studies, we were able to show that the III–V layers of nanocolumns obtained on porous silicon (por-Si) have not only a higher concentration of charge carriers as compared to layers grown on crystalline silicon (c-Si), but also a higher quantum yield photoluminescence (+25%).

Speaking about the efficiency of using a porous Si substrate instead of a crystalline one, it should be noted that, although the known attempts of growth on the porous layer [23] showed the promise of such an approach to the formation of integrated III–V/Si structures, in fact this did not lead to the development of the proposed technology. This is because in Ref. [23] the authors used layers of macro- and mesoporous silicon in the formation of a pliable substrate. As a result, research groups faced the fact that often the epitaxial film cracked, and it was not possible to overcome the difficulties associated with the creation of low-defect single-crystal solid solutions with a low dislocation density. In addition, the depth of the porous sublayer, the roughness and morphology of the surface were not controlled in any way, the issues of pre-epitaxial preparation of compliant substrates, as well as the processes of redistribution of stresses to the sublayer were not taken into account.

The results of our preliminary studies show that the growth of a GaN epitaxial film from nanocolumns on nanoporous Si substrates has a positive effect on the structural quality of epitaxial films and their thin structural properties. This, in turn, should certainly affect the electronic and optical properties exhibited by such structures, as well as the change in their stoichiometry.

In this regard, in the present work, using electron and optical spectroscopy, we studied the effect of a compliant Si substrate with a layer of nanoporous silicon (por-Si) previously formed on it on the epitaxial growth mechanisms of the self-ordered array of GaN nanocolumns and their subsequent coalescence in solid 2D layer.

2. Materials and research methods

GaN epitaxial layers were grown using PA MBE on a Veeco Gen 200 industrial type plant, which allows up to seven three-inch plates to be used simultaneously during one growth process. A high-frequency (13.56 MHz) plasma source Riber RFN 50/63 was used to activate nitrogen.

It should be noted that GaN layers grown on silicon substrates using PA MPE, as a rule, have a granular (mosaic) structure, due to the island mechanism of GaN nucleation on lattice-mismatched silicon substrates. In the process of growth, the growth of GaN nanoislands into nanocolumns and their coalescence into a continuous layer occur. At the same time, it is known that using PA MPE, it is possible to form both layers of GaN nanocolumns (in the case of nitrogen-enriched growth conditions) and relatively smooth layers (under metal-enriched conditions). In addition, the activation efficiency of molecular nitrogen at PA MPE does not depend on the substrate temperature, which allows changing the growth temperature of the GaN structures within wide limits, from extremely low to the maximum possible values for this technology (~900 °C).

For the growth of undoped GaN layers, Si(111) and por-Si(111) substrates were used, which underwent chemical preparation to remove organic contaminants. Immediately before the growth of the substrate, they were annealed in the growth chamber of PA MPE setup at the temperature T_s = 850 °C for 30 minutes. After that, the Si(111) substrates were nitrided at T_s = 850 °C for 30 minutes in a stream of activated nitrogen corresponding to an equivalent growth rate of GaN structures of about 0.1 μm h^{-1} to form a transition layer of silicon nitride on the Si(111) surface.

When creating a compliant por-Si substrate, a porous silicon layer was formed on a c-Si(111) single-crystal plate by electrochemical etching in an alcoholic solution of hydrofluoric acid according to the standard procedure [24–26]. The thickness of the porous layer was ~30 nm. The specified technological average pore size was ~1–5 nm.

The direct synthesis of GaN layers on nitrided Si(111) substrates consisted of two stages: first, an LT-GaN seed low-temperature layer 15 nm thick was grown at T_s = 650 °C and the gallium-activated nitrogen flow ratio was 1:1. After that, the main HT-GaN high-temperature layer ~820 nm thick was grown at T_s = 730 °C and the flow ratio was ~6:1. The element concentrations in the layers were determined more

precisely by means of X-ray microanalysis using an attachment to an electron microscope.

The carrier concentration and conductivity type were determined using the Hall effect by the van der Pauw method at room temperature using the Ecopia-3000 setup (Korea). Planar silver contacts with a thickness of 30 nm were deposited on films by magnetron sputtering. Studies of the phase composition of the surface by X-ray photoelectron spectroscopy (XPES) were performed on a laboratory spectrometer (SPECS GmbH) excited by the K_α line of Mg. Raman spectra were obtained on a Renishaw 1000 microscope with a $50^\times$ NPlan objective upon excitation by an argon laser radiation with a wavelength of 514.5 nm. Laser beam power does not exceed 3 mW.

The optical properties of the samples were studied in the wavelength range of 190–900 nm by UV spectroscopy using a PerkinElmer LAMBDA 650 system equipped with a universal URA attachment, which makes it possible to obtain reflection spectra in the range of angles of incidence 8°–80°.

3. Experimental results

3.1. Electrophysical measurements

Measurements of the conductivity type, concentrations, and carrier mobility by the van der Pauw method were carried out by us at room temperature. The experiment showed that the layer of GaN nanocolumns grown on both c-Si and por-Si substrates has p-type conductivity. Hall concentration of charge carriers and carrier mobility are shown in Table 1. It is clearly seen that the concentration of carriers for a film on crystalline silicon is higher, and the mobility of carriers is lower than for a layer grown on a por-Si substrate. The obtained results agree with the data already available for bulk GaN films [27, 28].

Table 1. The results of electrophysical methods of measuring the samples.

Sample	Carrier concentration/cm^{-3}	Mobility/ cm^2 V^{-1} s^{-1}
GaN/c-Si(111)	7.9×10^{19}	8.6
GaN/por-Si(111)	2.4×10^{18}	52.4

3.2. XPES measurement

Using the method of X-ray microanalysis, we determined the elemental composition of GaN films grown on two types of substrates. For the analysis, an accelerating voltage of 10 kV was used and sample areas of approximately 750×750 µm were studied. The effective depth of microanalysis was ∼0.25 µm. The experiment showed that the main elements in the film are gallium and nitrogen. It should be noted that the composition of the layer grown on a compliant por-Si(111) substrate is closer to the stoichiometric composition.

XPES analysis of the surface composition of GaN/Si(111) heterostructures at different depths, specified by the time of sample etching, was performed. The surface was etched for 30 s by argon ions with an energy of 4 keV at an ion current density of 30 A cm^{-2} and a sample etching rate of 1.5–2.5 nm min^{-1}. Thus, the depth of sample analysis using this technique was ∼1–2 nm.

The experimental data were processed using the Origin 9.0 software package. The method of determining the background line, as well as its subtraction according to the algorithms proposed by Shirley [9], was also implemented using this program. When finding the binding energies of the core levels of the heterostructure elements, the reference line was the C1s line of natural hydrocarbon contamination of the surface of any sample not subjected to special cleaning, reduced to the energy E_b[C 1s] = 285 eV. The identification of the core levels of elements and their chemical state based on the XPES results was carried out using the X-ray photoelectron spectra database of the US National Standards Institute.

Figure 1 shows the Ga $2p_{3/2}$ spectra of the samples studied. As a reference, a single-crystal GaN film with a thickness of 3 µm was used, obtained by MBE on an Al_2O_3 substrate using

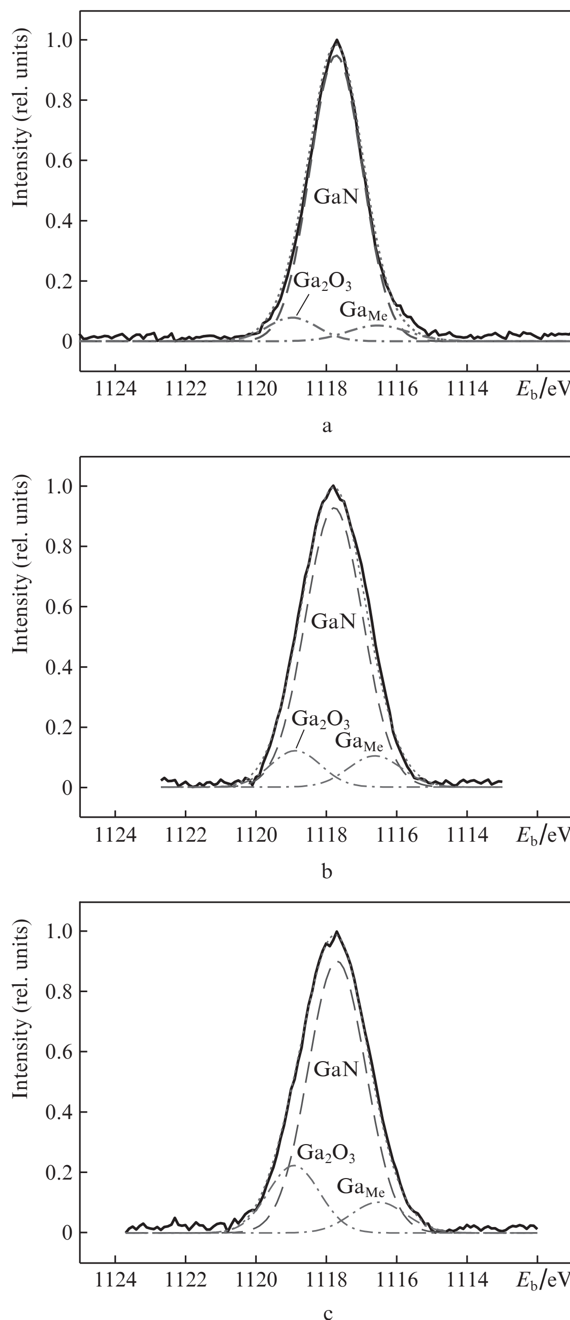

Figure 1. Ga $2p_{3/2}$ spectra of (a) the reference GaN sample and (b) GaN/c-Si(111) and (c) GaN/por-Si(111) heterostructures grown on crystalline and porous silicon. The solid curve is the experiment, the dotted curve is the model, and the dashed curve is GaN (reference).

standard technology that provides a high structural quality of a single-crystal GaN layer [29].

From the results of XPES analysis, it follows that the Ga 2p bands for the GaN layer grown on c-Si(111) and por-Si(111) are wider in both directions than the band for the reference GaN sample. In addition, the XPES spectra of the Ga 2p band for the GaN/c-Si(111) and GaN/por-Si(111) samples are generally the same.

The decomposition of all spectra of Ga 2p into components shows that the reference sample is mainly the GaN phase (the main peak corresponds to $E_b = 1178$ eV), while on its surface there may be a small amount of metallic gallium ($E_b = 1165$ eV) and oxide Ga_2O_3 ($E_b = 1119$ eV). As for the GaN layers grown on silicon substrates, the contribution of the side components to the decomposition of their experimental XPES spectra increases. The analysis shows that in the spectrum for a GaN layer grown on crystalline silicon, the component corresponding to metallic Ga (GaMe) is most pronounced. The N 1s spectra for the obtained samples practically do not differ from each other in the shape and position of the band and coincide with the spectrum for the GaN standard (E_b = 397.8 eV).

3.3. Optical research results

Figure 2 shows the Raman spectra of the studied samples obtained by the method we used [30]. From the experimental data, it can be seen that the spectra of both samples contain one set of combination modes. The most intense mode is the longitudinal optical phonon of a single crystal substrate Si (LO). In addition to this mode, in the Raman spectra there are three low-intensity vibrations near 430, 617 and 675 cm^{-1}, associated with Si. As to the response of the epitaxial layer, the spectra for both types of samples contain Gaussian-resolved E_1(TO) and A_1(LO) phonons for the GaN phase, located near ∼564 and 730 cm^{-1}, as well as an additional mode characteristic of wurtzite GaN in the region near 301 cm^{-1}.

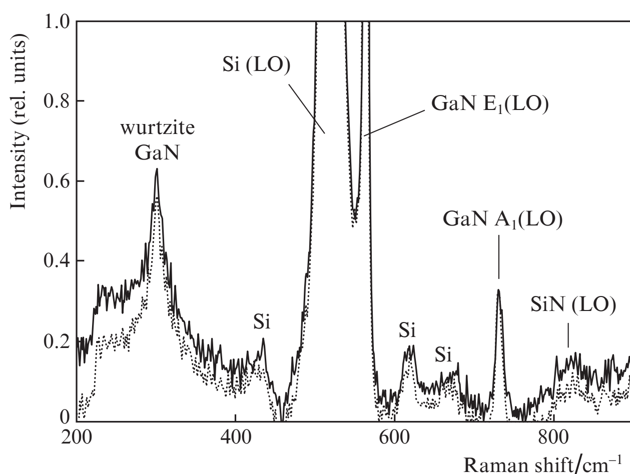

Figure 2. Results of Raman spectroscopy of (solid curve) GaN/c-Si(111) and (dotted curve) GaN/por-Si (111) heterostructures.

Attention should be paid to the fact that the position of the A_1(LO) mode in the spectrum for a heterostructure grown on a flexible por-Si substrate is shifted by 4 cm^{-1} relative to the position of this phonon in the Raman spectrum for the structure obtained on crystalline silicon. In addition, in the first case, the A_1(LO) mode has a smaller half-width. This is consistent with the X-ray diffraction data on the growth of a GaN layer, which is practically matched in terms of the lattice parameter with a porous sublayer in the growth plane and experiencing a significant distortion in the growth direction, but at the same time having a better crystalline quality than the layer obtained on the c-Si substrate.

Note that in the Raman spectra of both samples there is an additional low-intensity oscillation in the range of 820 cm^{-1}, which most likely can be attributed to the amorphous phase of silicon nitride SiN [31], which is formed as a result of unintended nitridation of the substrate at the initial stage of 3D heteroepitaxial growth of GaN. This result coincides with the previously obtained X-ray diffractometry data on the formation of an amorphous sublayer.

It should be noted that the frequencies of the main phonon modes determined by us experimentally for GaN in the Raman spectra do not coincide with the already available literature data for the bulk single-crystal layer [32]. It is well known that this occurs due to the appearance of biaxial deformation in the epitaxial layer due to the large mismatch of the lattice parameters in the GaN/Si heteropair. However, the frequency shift discovered by us agrees well with the results of the theory presented in [32–34], where the change in the optical phonon frequency in the spectrum is given by the following relationship:

$$\Delta\omega = 2a\varepsilon_{xx} + b\varepsilon_{zz}, \quad (1)$$

where a and b are the strain potentials of the crystal; and ε_{xx} and ε_{zz} are the components of the elastic tensor.

We investigated the optical properties of samples in the UV and visible ranges (190–900 nm) using the reflection imaging technique, which has already shown its efficiency in our previous studies of thin films formed on bulk substrates [35–38]. Using the proposed technique and the experimental reflection–transmission spectra of the sample obtained at different angles of incidence of radiation, the refractive index of the sample for the wavelength corresponding to the interference maximum/minimum can be calculated from the interference pattern, and the dispersion of the refractive index is determined in a wide wavelength range [36, 37].

For this aim, we use the relation between the thickness d of the epitaxial film grown on a thick substrate and the refractive index n:

$$d = \frac{N\lambda_1\lambda_2}{2(\lambda_1 - \lambda_2)\sqrt{(n^2 - \sin^2\alpha)}}. \quad (2)$$

Here, λ_1 and λ_2 are the wavelengths corresponding to the maximum and minimum interference in the spectrum; N is the interference order; and α is the angle of incidence of radiation on the film. In carrying out the calculation, we make the assumption that within the limits of wavelength variation, the refractive index changes only slightly.

Figure 3 presents the values of the refractive index of the samples studied, calculated on the basis of the proposed technique, as well as its approximated dispersion dependences. It is clearly seen that the refractive index of the epitaxial GaN layer grown on both the c-Si substrate and the compliant por-Si substrate monotonically increases with decreasing wavelength. In this case, in the wavelength range 330–430 nm (∼3.75–2.9 eV), an extreme increase in the refractive index is observed for both samples. This fact may indicate that the

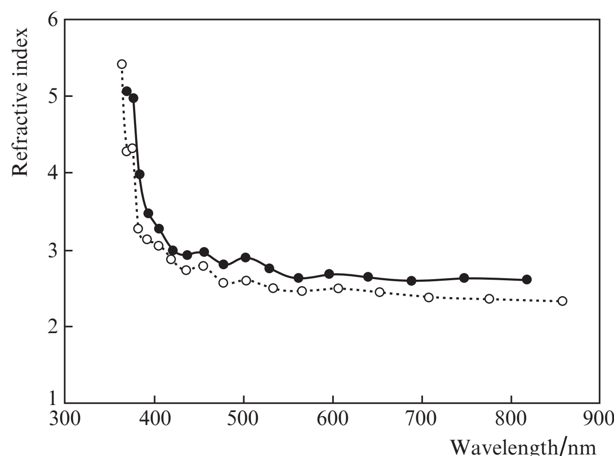

Figure 3. Dispersion dependence of the refractive index of (●) GaN/c-Si(111) and (○) GaN/por-Si(111) heterostructures.

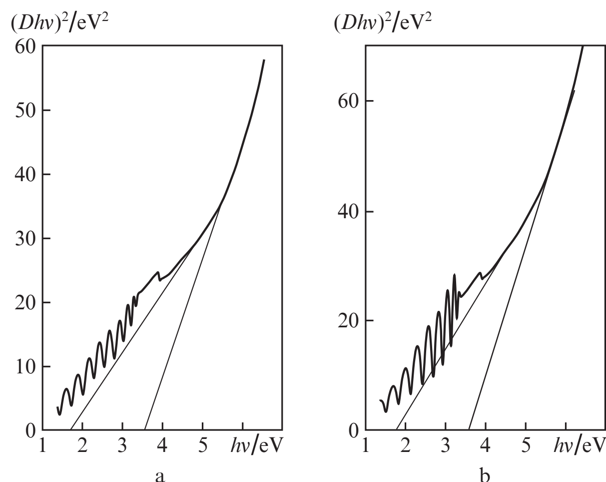

Figure 4. Dependences of $(Dh\nu)^2$ on the photon energy for samples of (a) GaN/c-Si(111) and (b) GaN/por-Si (111) heterostructures.

position of the fundamental absorption edge of the epitaxial film is close to the specified wavelength [39–41]. Note also that for the entire wavelength region where the dispersion of the refractive index of the GaN film was determined, a very important feature is characteristic: in the same spectral region, the refractive index of a GaN layer grown on a c-Si substrate is, on average, 10% higher than that obtained on a compliant por-Si substrate. In addition, based on the form of the dispersion function, it can be assumed that its greatest maximum (and hence the energy corresponding to the fundamental absorption edge) for the GaN/por-Si sample is shifted toward higher energies compared to the similar value for the GaN/c-Si sample, which should affect the mechanisms of optical absorption in the epitaxial GaN layer.

To reveal the features of optical absorption in samples, their experimental transmission spectra, obtained at an angle of electromagnetic radiation of ~67° in the wavelength range of 190–900 nm, were recalculated into absorption spectra.

Using the Kramers–Kronig relations [42], we calculated the optical density D of the samples and plotted the dependences $(Dh\nu)^2$ on the quanta energy $h\nu$ (Fig. 4). Graphical analysis of the results allows us to identify individual linear sections of these dependencies. Linear extrapolation of these areas to a zero energy value makes it possible to determine the energy of direct transitions characteristic of the studied samples (Table 2).

Analysis of the information obtained by us shows (Fig. 4) that the appearance of two direct transitions is characteristic of both samples. The first of them refers to direct allowed interband transitions between the Г_6V zone and the Г_1C zone of GaN. The energy of this transition practically coincides with the value of the optical band gap of GaN known from literature and is in good agreement with the data already available [43].

As for the second direct allowed transition with an energy of ~1.7 eV, its energy coincides with the band gap of the SiN compound. This result is consistent with X-ray diffraction and

Table 2. The results of X-ray analysis.

Sample	Energy of direct transitions/eV	
	Г_6V–Г_1C (GaN) [43]	zone–zone (SiN) [44]
GaN/c-Si(111)	3.55	1.76
GaN/por-Si(111)	3.58	1.77

Raman spectroscopy data on the formation of the amorphous phase of silicon nitride in the epitaxial film and with the results of our previous work [20].

It should be emphasised that the extrema of the refractive index dispersion dependence in the epitaxial GaN film grown on both c-Si and por-Si substrates agree well with the energies of the optical absorption edges determined from the $(Dh\nu)^2$ dependence on $h\nu$, as well as with data from the literature. This fact confirms our assumptions about the magnitude of the optical band gap for the epitaxial GaN layer grown by PA MBE on both types of substrates. In addition, we note that the optical band gap determined by us experimentally for the epitaxial GaN layer grown on a por-Si substrate is 0.1 eV higher than the value obtained for a single-crystal silicon layer.

4. Discussion of the results

Using PA MBE, integrated GaN/Si heterostructures were grown on Si(111) and por-Si(111) substrates. The spectroscopic analysis of the obtained samples was carried out. The study of the elemental composition of the surface layer of the GaN film showed that the composition of the layer grown on the compliant por-Si(111) substrate is closer to the stoichiometric one, and the formation of metallic gallium nanoclusters on its surface, which occurred during growth on the standard substrate c- Si, was not observed. In the same spectral region, the refractive index of the epitaxial GaN layer grown on a c-Si substrate is, on average, 10% larger than that obtained on a compliant por-Si substrate. In this case, the energy corresponding to the fundamental absorption edge for the GaN/por-Si sample is shifted toward higher energies in comparison with the similar value for the GaN/c-Si sample. Analysing our results, technological data, and information from already known literature sources, we would like to note that the temperature of growth significantly affects the size of the seed GaN islands, since with its increase the surface mobility of adatoms of the deposited substance significantly increases [45]. The higher the surface mobility, the larger the average size of the emerging seed islands until their complete coalescence. However, in this context, we can speak only about the average grain size during the formation of GaN nanofibres, since the real distribution of their size is rather chaotic. In Ref. [46], it was shown that the {111} plane is the most energetically

favourable crystallographic plane in silicon for the nucleation of GaN. At the initial stage, we assume that selective etching in this plane when creating a por-Si sublayer leads to the formation of a surface morphology described in [47], which consists of isotropically distributed GaN hillocks. When the thickness of the porous layer is 20 nm, the hillocks are approximately the same size and are truncated, and their upper plane corresponds to the {111} silicon crystallographic plane. Thus, the nucleation of GaN on the planes of truncated etched hillocks is energetically favourable, and the high surface mobility of adatoms leads to the fact that each single seed island completely covers the corresponding {111} plane of each hillock. We believe that the use of a low-temperature buffer layer with 3D surface morphology leads to the removal of stresses generated at the GaN-Si(111) interface on the lateral free surfaces of the nanocolumns. The use of the nanoporous por-Si layer makes it possible to reduce the density of seed dislocations by reducing the angular and planar misorientations of the seed islands, which consequently reduces the generation of misfit dislocations.

5. Conclusions

Integrated heterostructures based on the self-ordered array of GaN nanocolumns on Si substrates with a sufficiently uniform diameter distribution, subsequently coalescing into a 2D layer, were obtained using PA MBE.

The use of a compliant por-Si substrate for the synthesis of GaN by PA MBE made it possible to obtain a crack-free GaN layer, which had a positive effect on its optical properties in the UV region.

In the same spectral region, the refractive index of the epitaxial GaN layer grown on a c-Si substrate is, on average, 10% larger than that obtained on a compliant por-Si substrate. In this case, the energy corresponding to the fundamental absorption edge of the GaN/por-Si sample is shifted toward higher energies in comparison with the similar value for the GaN/c-Si sample, which indicates a larger optical width of the band gap on the por-Si substrate.

The use of a compliant por-Si substrate, the procedure of pre-epitaxial high-temperature nitridation of this substrate, and the technological conditions under MBE PA, which ensured the nucleation of the GaN layer in the 3D growth mode with a subsequent transition to the 2D growth mode of the GaN layer, made it possible to avoid the Ga-Si etching process and provide a sharp smooth interface Si-GaN. It also allowed partial suppression of the generation of tensile stresses arising when the heterostructure is cooled from growth temperature to room temperature by its relaxation at the Si-GaNn nanoporous interface.

Thus, the use of compliant Si-substrates is convenient for the formation of GaN-based semiconductor device heterostructures using PA MBE.

Acknowledgements. This work was supported by the RF President's Grants Council (Grant MD-42.2019.2) and the Government of the Russian Federation (Decree No. 211, Contract No. 02.A03.21.0006). Growth experiments were carried out in the framework of the State task of the Ministry of Education and Science of the Russian Federation (No. 16.9789.2017/BC). In part of diagnostics of integrated structures, the work was supported by the Ministry of Education and Science of the Russian Federation (Grant No. 11.4718.2017/8.9) in the framework of the State Task to Universities in the Field of Research Activity for 2017–2019. In part of properties of compliant substrates, the work was performed in accordance with the State Task of the Ioffe Institute. We are deeply grateful to the staff of the Laboratory of Nano- and Microtechnologies of the Karlsruhe Research Centre for providing access to the instruments of laboratories.

References

1. Ho V.X., Al Tahtamouni T.M., Jiang H.X., Lin J.Y., Zavada J.M., Vinh N.Q. *ACS Photonics*, **5**, 1303 (2018).
2. Laurent T., Manceau J.-M., Monroy E., Lim C.B., Rennesson S., Semond F., Julien F.H., Colombelli R. *Appl. Phys. Lett.*, **110**, 131102 (2017).
3. Ajay A., Lim C.B., Browne D.A., Polaczynski J., Bellet-Amalric E., den Hertog M.I., Monroy E. *Phys. Status Solidi B*, **254**, 1600734 (2017).
4. Wang W., Wang H., Yang W., Zhu Y., Li G. *Sci. Rep.*, **6**, 24448 (2016).
5. Derluyn J., Germain M., Meissner E., in *Gallium Nitride-Enabled High Frequency High Efficiency Power Conversion* (Cham: Springer, 2018) pp 1–28.
6. Li D. *Sci. Bull.*, **61**, 1723 (2016).
7. Gkanatsiou A., Lioutas C.B., Frangis N., Polychroniadis E.K., Prystawko P., Leszczynski M. *Superlattices Microstruct.*, **103**, 376 (2017).
8. Sugawara Y., Ishikawa Y., Watanabe A., Miyoshi M., Egawa T. *J. Cryst. Growth.*, **468**, 536 (2017).
9. Buzynin Y., Shengurov V., Zvonkov B., Buzynin A., Denisov S., Baidus N., Drozdov M., Pavlov D., Yunin P. *AIP Adv.*, **7**, 015304 (2017).
10. Yuan Kok I.J., Soh C.B., Sang N.X., Lee T.H., Kadir A., Chua S.J. *Procedia Eng.*, **215**, 1 (2017).
11. Damilano B., Natali F., Brault J., Huault T., Lefebvre D., Tauk R., Frayssinet E., Moreno J.-C., Cordier Y., Semond F., Chenot S., Massies J. *J. Appl. Phys. Express*, **1**, 121101 (2008).
12. Li K.H., Fu W.Y., Cheung Y.F., Wong K.K.Y., Wang Y., Lau K.M., Choi H.W. *Optica*, **5**, 564 (2018).
13. Li C., Ji Z., Li J., Xu M., Xiao H., Xu X. *Sci. Rep.*, **7**, 15301 (2017).
14. Zhang W., Zhang X., Wang Y., Hu F. *Opt. Mater.*, **72**, 422 (2017).
15. Kano T., Yoshida J., Miyagawa R., Mizuno Y., Oto T., Kishino K. *Electron. Lett.*, **51**, 2125 (2015).
16. Vanhollebeke K., Moerman I., Van Daele P., Demeester P. *Prog. Cryst. Growth Charact. Mater.*, **41**, 1 (2000).
17. Hahn C., Zhang Z., Fu A., Wu C.H., Hwang Y.J., Gargas D.J., Yang P. *ACS Nano*, **5**, 3970 (2011).
18. Wang H.-C., Tang T.-Y., Yang C.C., Malinauskas T., Jarasiunas K. *Thin Solid Films*, **519**, 863 (2010).
19. Bougrioua Z., Gibart P., Calleja E., Jahn U., Trampert A., Ristic J., Utrera M., Nataf G. *J. Cryst. Growth*, **309**, 113 (2007).
20. Seredin P.V., Goloshchapov D.L., Lenshin A.S., Mizerov A.M., Zolotukhin D.S. *Phys. E: Low-Dimens. Syst. Nanostructures*, **104**, 101 (2018).
21. Seredin P.V., Lenshin A.S., Zolotukhin D.S., Arsentyev I.N., Zhabotinskiy A.V., Nikolaev D.N. *Phys. E: Low-Dimens. Syst. Nanostructures*, **97**, 218 (2018).
22. Seredin P.V., Lenshin A.S., Zolotukhin D.S., Arsentyev I.N., Nikolaev D.N., Zhabotinskiy A.V. *Phys. B: Condens. Matter.*, **530**, 30 (2018).
23. Romanov S.I., Mashanov V.I., Sokolov L.V., Gutakovskii A., Pchelyakov O.P. *Appl. Phys. Lett.*, **75**, 4118 (1999).
24. Lenshin A.S., Seredin P.V., Agapov B.L., Minakov D.A., Kashkarov V.M. *Mater. Sci. Semicond. Process.*, **30**, 25 (2015).
25. Len'shin A.S., Kashkarov V.M., Seredin P.V., Agapov B.L., Minakov D.A., Tsipenyuk V.N., Domashevskaya E.P. *Tech. Phys.*, **59** (2), 224 (2014) [*Zh. Tekh. Fiz.*, **84** (2), 70 (2014)].
26. Kashkarov V.M., Len'shin A.S., Seredin P.V., Agapov B.L., Tsipenuk V.N. *J. Surf. Invest.: X-Ray Synchrotron Neutron Tech.*, **6**, 776 (2012).

27. Usikov A., Kovalenkov O., Ivantsov V., Sukhoveev V., Dmitriev V., Shmidt N., Poloskin D., Petrov V., Ratnikov V. *MRS Symp. Proc.*, **831**, 453 (2005).
28. Lieten R.R., Motsnyi V., Zhang L., Cheng K., Leys M., Degroote S., Buchowicz G., Dubon O., Borghs G. *J. Phys. Appl. Phys.*, **44**, 135406 (2011).
29. Mizerov A.M., Jmerik V.N., Kaibyshev V.K., Komissarova T.A., Masalov S.A., Ivanov S.V. *Semiconductors*, **43**, 1058 (2009).
30. Seredin P.V., Glotov A.V., Domashevskaya E.P., Arsentyev I.N., Vinokurov D.A., Tarasov I.S. *Phys. B: Condens. Matter*, **405**, 2694 (2010).
31. San Andrés E., del Prado A., Martínez F.L., Mártil I., Bravo D., López F.J. *J. Appl. Phys.*, **87**, 1187 (2000).
32. Correia M.R., Pereira S., Pereira E., Frandon J., Alves E. *Appl. Phys. Lett.*, **83**, 4761 (2003).
33. Briggs R.J., Ramdas A.K. *Phys. Rev. B*, **13**, 5518 (1976).
34. Teng L., Zhang R., Xie Z.-L., Tao T., Zhang Z., Li Y.-C., Liu B., Chen P., Han P., Zheng Y.-D. *Chin. Phys. Lett.*, **29**, 027803 (2012).
35. Volodin V.A., Efremov M.D., Prince V.Ya., Preobrazhensky V.V., Semyagin B.R., Govorov A.O. *JETP Lett.*, **66** (1), 47 (1997) [*Pis'ma Zh. Eksp. Teor. Fiz.*, **66** (1), 45 (1997)].
36. Seredin P.V., Lenshin A.S., Kashkarov V.M., Lukin A.N., Arsentiev I.N., Bondarev A.D., Tarasov I.S. *Mater. Sci. Semicond. Process.*, **39**, 551 (2015).
37. Seredin P.V., Kashkarov V.M., Arsentyev I.N., Bondarev A.D., Tarasov I.S. *Phys. B: Condens. Matter*, **495**, 54 (2016).
38. Seredin P.V., Lenshin A.S., Goloshchapov D.L., Lukin A.N., Arsentyev I.N., Bondarev A.D., Tarasov I.S. *Semiconductors*, **49**, 915 (2015).
39. Kuzmenko A.B. *Rev. Sci. Instrum.*, **76**, 83 (2005).
40. Lucarini V., Peiponen K.-E., Saarinen J.J., Vartiainen E.M. *Kramers– Kronig Relations in Optical Materials Research* (Berlin – New York: Springer, 2005).
41. Seredin P.V., Goloschapov D.L., Lukin A.N., Len'shin A.S., Bondarev A.D., Arsent'ev I.N., Vavilova L.S., Tarasov I.S. *Semiconductors*, **48**, 1527 (2014).
42. Ukhanov I.I. *Opticheskiye svoystva poluprovodnikov* (Optical Properties of Semiconductors) (Moscow: Nauka, 1977).
43. Specht P., Ho J.C., Xu X., Armitage R., Weber E.R., Erni R., Kisielowski C. *Solid State Commun.*, **135**, 340 (2005).
44. Deshpande S.V., Gulari E., Brown S.W., Rand S.C. *J. Appl. Phys.*, **77**, 6534 (1995).
45. Nechaev D.V., Aseev P.A., Jmerik V.N., Brunkov P.N., Kuznetsova Y.V., Sitnikova A.A., Ratnikov V.V., Ivanov S.V. *J. Cryst. Growth.*, **378**, 319 (2013).
46. Lee S.C., Sun X.Y., Hersee S.D., Brueck S.R.J., Xu H. *Appl. Phys. Lett.*, **84**, 2079 (2004).
47. Houbertz R., Memmert U., Behm R.J. *J. Vac. Sci. Technol. B: Microelectron. Nanometer Struct. Process. Meas. Phenom.*, **12**, 3145 (1994).